Calculated and measured transmittance of a tunable metallic photonic crystal filter for terahertz frequencies

Timothy D. Drysdale

Department of Electronics and Electrical Engineering,

University of Glasgow, Glasgow, G12 8LT, United Kingdom

Richard J. Blaikie

MacDiarmid Institute for Advanced Materials and Nanotechnology,

Department of Electrical and Computer Engineering,

University of Canterbury, Private Bag 4800, Christchurch, New Zealand

David R. S. Cumming*

Department of Electronics and Electrical Engineering,

University of Glasgow, Glasgow, G12 8LT, United Kingdom

Abstract

A tunable metallic photonic crystal filter with a mechanical tuning mechanism is demonstrated. The performance is predicted with rigorous full-vector electromagnetic simulations (finite-difference time-domain). A prototype has been built and characterized in the W-band (70 – 110 GHz) using a vector network analyzer configured for free-space measurement of S-parameters. The measured filter's pass band has a quality factor of 11, a tuning range of 3.5 GHz and insertion loss of only 1.1 to 1.7 dB. Device fabrication is straightforward, yielding an inexpensive, robust and compact tunable filter.

Tunable spectral filters are expected to find use in emerging terahertz frequency applications such as spectroscopy, imaging and communications, just as they have in other regions of the electromagnetic spectrum. However, existing technologies targeted for the visible[1] or infrared[2,3] may be unsuitable, or difficult to fabricate, for the longer terahertz wavelengths. Furthermore, microwatt power levels[4] may pose problems for devices that suffer from substrate losses. Metallic photonic crystal filters are a promising alternative, and have the advantage of being compact, robust and inexpensive. However, the few tuning schemes that are known may not be suitable in all applications[5,6].

In this Letter, we report the design and demonstration of a mechanically-tunable metallic photonic crystal filter designed for free-space terahertz frequency operation. The basic component of the filter is a metal plate comprising two orthogonal linear grids with integral mounting lugs as shown in Fig. 1(a) (not to scale). The filter is constructed by stacking two such plates to give the device cross section shown in Fig. 1(b) (lugs omitted). Linearly-polarized plane-waves are normally incident from above, with the electric field, $\mathbf{E}$, oriented as shown (the orthogonal linear polarization is blocked). All the rods in the grids are of subwavelength size, having dimensions of width r, depth d, and period Λ. The inner two grids are initially aligned, and an allowance is made for a small fixed separation, g, between the plates.

The transmission characteristic of this device exhibits a plasmon-like forbidden band that extends from zero frequency up to a cut-off frequency, f_c, where the associated wavelength, λ_c, is approximately equal to the twice the lattice constant of the 3-D metallic grid structure[7] ($\lambda_c \approx 2\Lambda$). There is a single-peaked transmission band located just above the cutoff frequency, associated with the single layer of micro-cavities formed in the center of the device[8]. Since most metals may be treated as perfect electrical conductors at microwave

and terahertz frequencies[9], the peak transmission should be 0 dB.

The center frequency of the transmission peak is tuned by a relative lateral shift, $0 < s < \Lambda/2$, of the plates in a direction parallel to the inner grid's grating vector, $\mathbf{K}$, as shown in Fig. 1(c). The plate separation g is not used to tune the device, and therefore the tuning method is different to Fabry-Pérot cavity-based techniques[6,10]. Two competing tuning mechanisms exist. First, for $s < r$ the rods of the inner grids overlap, and the strong capacitive coupling influences the frequency, f_p, of the transmission peak according to $f_p = 1/\left(2\pi\sqrt{LC}\right)$ where L is the inductance and C the capacitance of the device[11]. As s increases, the rod overlap reduces and there is less area in direct contact between the plates. This increases the effective area of the plates that is capacitively coupled, increasing C and lowering the peak frequency. Simple electrostatic modelling of these structures supports this assertion. For wholly-dielectric grating couplers[12], the peak frequency continues to fall until the maximum tuning shift is reached ($s = \Lambda/2$), but for this metallic photonic crystal structure a second mechanism becomes dominant. The resonant characteristics of the micro-cavities dominate the tuning characteristics once the inner rods are no longer overlapped ($s > r$), at which point the peak's center frequency begins to rise again due the reduction of the effective cavity size.

Above the first transmission band lies the second (true) photonic band gap[8], and into this gap there is introduced a defect mode resonance if there are any disturbances to the regular periodicity of the crystal. A defect mode resonance is expected for shift positions that result in asymmetric spacing of the inner grids ($s \neq 0, \Lambda/2$). We note that the structure has a simple tetragonal unit cell and that the direction of propagation is in the stacking direction, although there is only one layer in the stack. For this reason, we are primarily interested in the transmittance of the device, rather than the entire photonic band structure.

For operation in the W-band (70 – 110 GHz, $2.7 < \lambda_0 < 4.2$ mm), the following dimensions were chosen: $\Lambda = 1.8$mm, $r = 450\mu$m, $d = 500\mu$m. These dimensions can be adjusted to fine tune the filter properties or accommodate fabrication constraints, or scaled for operation at other microwave and terahertz frequencies.

The expected performance of a prototype was quantified using a Finite-Difference Time-Domain (FDTD) analysis method. An infinitely wide grid was modeled by surrounding a single unit cell of the device with periodic boundary conditions[13]. The frequency response of the filter was determined with 0.53 GHz resolution by Gaussian pulsed excitation and FFT of the transmitted fields. The plate separation was set to the minimum non-zero distance (one simulation cell), giving $g = 30$ μm. Nine different tuning positions in the range $0 < s < 900$ μm ($0 < s < \Lambda/2$) were simulated.

A prototype device with an area of 34 mm by 30 mm (excluding the lugs) was constructed from 1 mm thick 5251 aluminum alloy sheet using conventional milling techniques. The plates were mounted on Tufnel holders between 20 mm $\times$ 20 mm square apertures of absorbing foam, and actuated by a three-axis translation stage and differential micrometers. Some inhomogeneity in the plate separation was observed, with g typically 10 μm. An anechoic environment was created by covering nearby reflective surfaces with absorbing foam. Full 2-port complex S-parameter measurements were taken using a Wiltron 360B vector network analyzer along with two WR-10 standard gain horn antenna, Wiltron SM4873 transmission-reflection measurement units and a Wiltron 61878B sweep synthesizer, giving -15dBm output power at 67 – 110 GHz after mixing. A schematic of the experimental setup is presented in Fig. 2. A line-reflect-line calibration was performed, then the horns were added and a reference measurement was taken of the entire experimental setup including a dummy filter with the gridded area missing. Fabry-Pérot resonances arising from multiple

reflections between the horns and the filter were averaged out by taking 15 measurements at different horn spacings of 60 – 65 mm. The device was measured at each of the nine tuning positions for which simulations were performed.

The calculated and measured transmission characteristics of the filter are plotted in Fig. 3 for the tuning positions that yield the highest and lowest center frequency for the transmission peak, with simulated results in Fig. 3(a) and measured results in Fig. 3(b). Examining Fig. 3(a), the transmission peak t_1 shows tuning over a 9.5 GHz range for a shift of $s = 360$ μm, giving a tuning sensitivity of 26 GHz/mm. The maximum predicted transmission of peak t_1 is -0.1 dB, with 0 dB not being observed due to the frequency resolution of the FFT, while the defect mode resonance t_2 is predicted to peak at -3.8 dB. The quality factor (Q) of the peaks varies from 21 – 31 for t_1 and is 125 for t_2. The measured device performs similarly, with measured peaks m_1 and m_2 corresponding to the simulated peaks t_1 and t_2 except for a slight change in tuning shift. The tuning range shown by peak m_1 is lower than predicted, at 3.5 GHz, giving a tuning sensitivity of 15 GHz / mm. We attribute the reduced tuning range to the fact that the rod widths in the machined device are approximately 270 μm whereas the original specification was for 450 μm (this is simply a machining tolerance). When we modify the simulations to accommodate this mismatch we find a much closer agreement between simulation and measurement.

This peak is slightly lossier than predicted, with the loss varying from -1.1 to -1.7 dB, while the defect mode resonance peak is at -7.4 dB. The loss is attributed to the finite conductivity of the plates, although there may also be a contribution from a systematic error in de-embedding the loss of the free-space measurement setup. The stop band attenuation is >10 dB, in good agreement with the simulations. The Q of the measured peaks is also lower at 11 and 17 for peaks m_1 and m_2 respectively. The reduced Q observed in the measurements

is attributed to the angular sensitivity of f_p[14] in conjunction with the $\sim 6^\circ$ range of incident angles arising from the use of standard-gain horn antenna.

The center frequency of the main peak and the defect mode resonance are plotted against tuning shift in Fig. 4 for the measured device and both simulated devices. The two regimes of the main peak's tuning characteristic are evident, as is the near-linear tuning of the defect mode resonance. The capacitive-coupling mechanism dominates the transmission-peak tuning for shifts $0 < s < 360$ μm (simulation t1, $r = 450$ μm) and $0 < s < 240$ μm (simulation t1a, $r = 270$ μm, and measurement m1), while the other mechanism dominates at larger shifts. Strong capacitive coupling is observed over a reduced range of separations in the measured device due to the smaller rod width. At larger shifts, the rod width is less critical, but the tuning sensitivity is reduced to 6 GHz / mm (simulation t1, $r = 450$ μm), 5 GHz / mm (measurement m1) and 1.7 GHz / mm (simulation t1a, $r = 270$ μm).

Defect mode resonances appear as expected for all shifts $s \neq 0, \Lambda/2$ and give a near-linear tuning range of 12 GHz for a sensitivity of 18 GHz / mm in simulations with $r = 450$ μm (t2). The measured defect mode resonances (m2) appear 7 GHz lower than predicted due to the already mentioned dimensional tolerances, but show the same near-linear tuning response with a tuning range of 11.7 GHz and sensitivity of 21 GHz / mm. The simulations for the device with the small rod width ($r = 270$ μm) (t2a) show defect mode resonances with a tuning range 10.7 GHz and a sensitivity of 18.8 GHz / mm, but at 5 GHz lower than the measured data.

The performance is sensitive to the separation g between the plates. For a simulated device with $r = 450$ μm, results not shown here indicate a maximum tuning range for the transmission peak of 13.4 GHz in the ideal case ($g = 0$), reducing to 9.5 GHz for $g = 30$ μm and 9.0 GHz for $g = 60$ μm. The separation should therefore be minimized in an optimal

device.

In conclusion, a tunable metallic photonic crystal filter has been designed and successfully demonstrated in good agreement with simulations. The pass band has a Q of 11, a tuning range of 3.5 GHz, a tuning sensitivity of 15 GHz/mm and maximum transmission in the range -1.1 to -1.7 dB. Fabrication is straightforward, yielding an inexpensive, robust and compact tunable filter. Simulations suggest there is room for improvement.

This work has been supported by Scottish Enterprise's Proof of Concept Fund.

* Author to whom all correspondence should be addressed; electronic mail: d.cumming@elec.gla.ac.uk

[1] P. Bondavalli, R. LeDantec, and T. Benyattou, J. Microelectromech. Syst. **10**, 298 (2001).

[2] G. Lammel, S. Schweizer, S. Schiesser, and P. Renaud, J. Microelectromech. Syst. **11**, 815 (2002).

[3] H. Alause, J.P. Malzoc, F. Grasdepot, V. Nouaze, J. Hermann, and W. Knap, IEE Proc. Optoelectronics **144**, 350 (1997).

[4] P. Siegel, IEEE Trans. Microwave Theory Tech. **50**, 910 (2002).

[5] J.-M. Lourtioz, A. de Lustrac, F. Gadot, A. Chelnokov, T. Brillat, A. Ammouche, J. Danglot, O. Vanbésien, and D. Lippens, J. Lightwave Tech. **17**, 2025 (1999).

[6] B. Temelkuran, H. Altug, and E. Ozbay, IEE Proc. Optoelectronics **145**, 409 (1998).

[7] D.F. Sievenpiper, M.E. Sickmiller, and E. Yablonovitch, Phys. Rev. Lett. **76**, 2480 (1996).

[8] F. Gadot, A. de Lustrac, J.-M. Lourtioz, T. Brillat, A. Ammouche, and E. Akmansoy, J. Appl. Phys. **85**, 8499 (1999).

[9] S. Fan, P.R. Villeneuve, and J. D. Joannopoulos, Phys. Rev. B **54**, 11245 (1996).

[10] R. Ulrich, T. J. Bridges, and M. A. Pollack, Appl. Opt. **9**, 2511 (1970).

[11] D.F. Sievenpiper, E. Yablonovitch, J.N. Winn, S. Fan, P.R. Villenueve, and J.D. Joannopoulos, Phys. Rev. Lett. **80**, 2829 (1998).

[12] W. Nakagawa and Y. Fainman, In Diffractive Optics & Micro Optics, Tucson, Arizona, 3 – 6 June 2002.

[13] A. Alexanian, N. J. Kolias, R. C. Compton, and R. A. York, IEEE Microwave Guid. Wave

Lett. **6**, 138 (1996).

[14] W. Nakagawa, P.-C. Sun, C.-H. Chen and Y. Fainman, Opt. Lett. **27**, 191 (2002).

List of Figure Captions

Fig. 1. (a) One of two metal plates required to make the filter. Each plate is made from a single piece of aluminum. (b) The cross section through the device with two plates. (c) Tuning is achieved by a lateral shift s of one plate parallel to the inner grids' grating vector $\mathbf{K}$. The plate separation g is not used to tune the device, and is ideally zero.

Fig. 2. The measurement setup includes two horn antenna, a vector network analyzer and associated equipment.

Fig. 3. Frequency spectra of the filter prototype at the tuning positions that yield the highest and lowest center frequency for the transmission peak. (a) Simulated $s = 0, 360$ μm; (b) measured $s = 0, 240$ μm.

Fig. 4. Plot of the simulated (two devices) and measured center frequency of the transmission peak and the defect mode resonance as a function of tuning shift s. Note that t1, t2, m1 and m2 are as defined in Fig. 3, while t1a and t2a are simulations from a device with $r = 270$ μm.

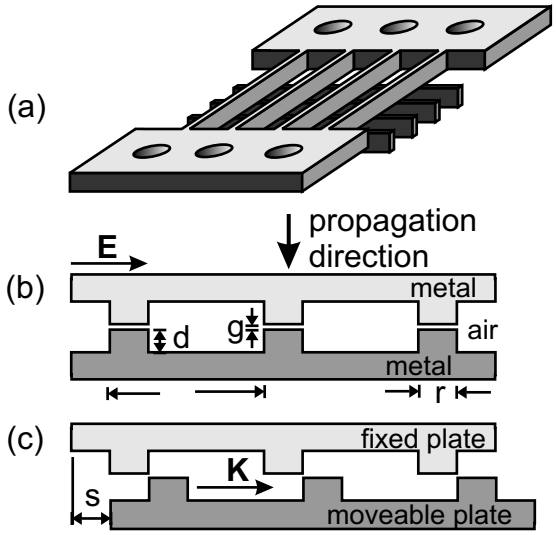

FIG. 1: Drysdale et. al., *Applied Physics Letters*

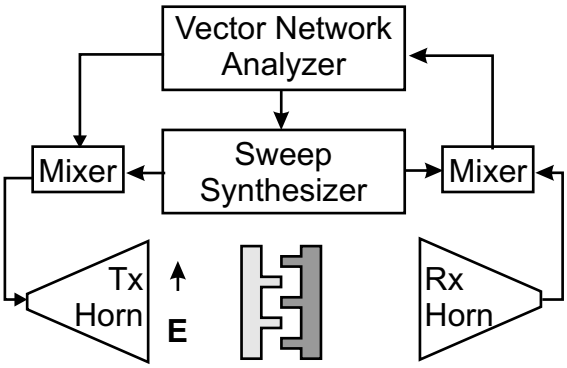

FIG. 2: Drysdale et. al., *Applied Physics Letters*

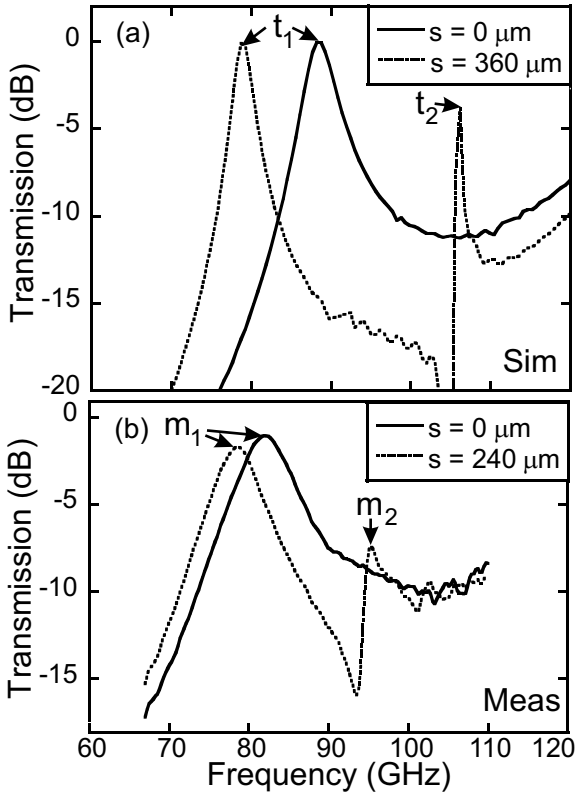

FIG. 3: Drysdale et. al., *Applied Physics Letters*

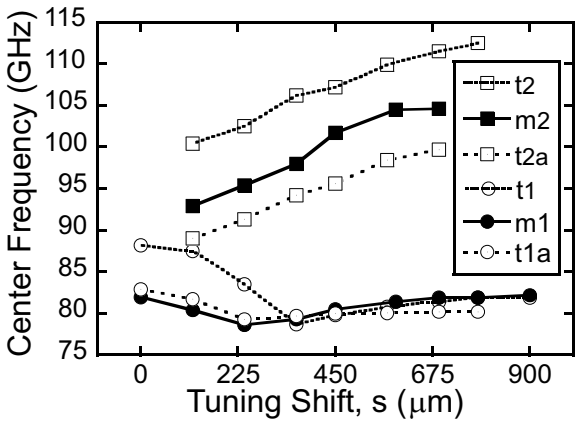

FIG. 4: Drysdale et. al., *Applied Physics Letters*